Clays and Clay Minerals, Vol. 53, No. 2, 171–178, 2005.

MODELING THE RESPONSE OF PYROPHYLLITE INTERLAYER TO APPLIED STRESS USING STEERED MOLECULAR DYNAMICS

DINESH R. KATTI*, STEVEN R. SCHMIDT, PIJUSH GHOSH AND KALPANA S. KATTI
North Dakota State University, Department of Civil Engineering, Fargo, ND 58105, USA

Abstract—Pyrophyllite is the precursor to other smectite-group minerals which exhibit swelling. The mineral structure of pyrophyllite can lead to other minerals in the smectite group, including montmorillonite, through appropriate isomorphous substitutions. In this work, an atomic model of the pyrophyllite interlayer was constructed. The response of the interlayer was evaluated using steered molecular dynamics simulations. In steered molecular dynamics, external forces were applied to individual atoms to study the response of the model to applied forces. In this work, forces are applied to the surface clay atoms to evaluate the displacement *vs.* applied stress in the interlayer between clay layers. This paper describes the construction of the model, the simulation procedure, and the results of the simulations which show that under the applied loading, deformation occurs mainly in the interlayer. The clay layers show relatively little deformation. The results show that the relationship between applied stress and displacement of the interlayer is linear. The stress-deformation relationship for the interlayer is presented.

Key Words—Interlayer Spacing, Molecular Dynamics, Pyrophyllite.

INTRODUCTION

Clays are materials of importance in geotechnical and geoenvironmental engineering, in the field of nanocomposites, and in the petroleum industry. Understanding the interaction between clay and water or other fluids is important in the use of these materials. Current literature indicates that understanding molecular interactions is necessary for modeling clay swelling. The volume of bound water and the interaction between particles has been described in the context of the diffuse double layer using the Stern-Guoy theory. However, this theory has significant limitations and does not accurately describe interlayer expansion and swelling of montmorillonites (Jo *et al.*, 2001). Likewise, another commonly used theory, the osmotic swelling model, fails to explain clay swelling quantitatively (McBride, 1994). Discrete element models have been successful in predicting the properties of kaolinite but to a limited extent only for montmorillonite (Anderson and Lu, 2001; Chen *et al.*, 2000). Previous work has shown that as clay swells, the particles break apart (Katti and Shanmugasundaram, 2001). In order to describe the evolution of microstructure in swelling clays accurately, it is necessary to model the clay-water interactions in the interlayer quantitatively using steered molecular dynamics.

Many molecular dynamics (MD) studies for rigid clay layers (Chang *et al.*, 1995, 1998; Greathouse *et al.*, 2000; Shroll and Smith, 1999; Smith, 1998; Capkova *et al.*, 1998; Karaborni *et al.*, 1996) and for flexible clay layers (Hwang *et al.*, 2001; Newman *et al.*, 2002; Teppen *et al.*, 1997; Warne *et al.*, 2000) have been published recently. The model described in this work uses flexible clay layers to derive the mechanical properties of pyrophyllite layers and its interlayer.

Pyrophyllite is a fundamental structure to all smectite-group clays. Having no water molecules or cations in the interlayer, pyrophyllite serves as a good measure of the response obtained purely from the interaction of the clay segments. Through this study, the mechanical properties of the clay layers can be compared with those of the interlayer. Because of the relative simplicity of pyrophyllite, direct conclusions cannot be made about the behavior of the interlayer of other smectite-group clays. However, the behavior of the crystalline clay layers can give a reasonable approximation of other smectites.

MODELING APPROACH

The clay molecule is most commonly referred to as a layer (Klein, 2002). The void space between clay layers, frequently occupied by water and cations, is known as the interlayer. When interlayer spacing is maintained by external forces, the applied forces can be assumed to be equal to the interlayer swelling pressure. Swelling *vs.* swelling pressure of the interlayer can then be evaluated by reducing the externally applied stress and measuring the corresponding interlayer spacing. The model of dry pyrophyllite is considered to be as shown in Figure 1. In this model, the deformation of the interlayer and clay layers can be studied under externally applied loads. To perform this study, MD in the isobaric-isothermal ensemble (constant NPT) was applied. Forces of gradually increasing magnitude were applied in each

* E-mail address of corresponding author:
dinesh.katti@ndsu.nodak.edu
DOI: 10.1346/CCMN.2005.0530207

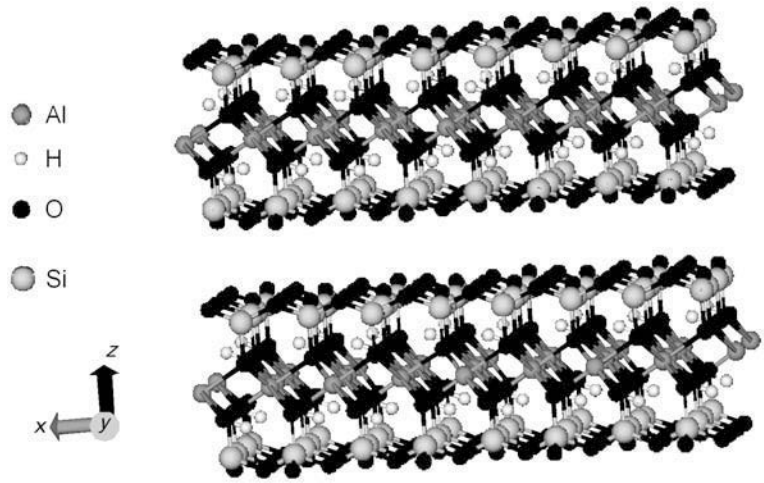

Figure 1. Perspective view of two pyrophyllite layers comprising 2 × 4 unit-cells each.

simulation and the resulting deformations of the interlayer and clay layers are found.

This work seeks to evaluate quantitatively the interactive forces existing in the interlayer between two clay layers. To accomplish this, opposing forces were applied to the surface of dry pyrophyllite as shown in Figure 2. The forces examined included 0, 0.001, 0.01, 0.1, 1, 2, 4, 5, 7, 10, 12, 15, 17, 20, 30, 50, 70, 100, 120, 140 and 160 pN (equivalent to stresses of 0, 0.00001, 0.0001, 0.001, 0.01, 0.02, 0.04, 0.05, 0.07, 0.10, 0.12, 0.16, 0.18, 0.21, 0.31, 0.52, 0.73, 1.04, 1.24, 1.45 and 1.66 GPa, respectively). The interlayer distance was measured after the force had been applied and the simulation had come to equilibrium. This was done by tracking the coordinates of atoms in the central region of the model. A relationship between stress and interlayer spacing was developed. Also a stress *vs*. 'interlayer strain' relationship is presented for the interlayer region, which is analogous to the stress-strain relationship for solids.

MODEL CONSTRUCTION

Pyrophyllite has the chemical formula $Al_2Si_4O_{10}(OH)_2$ (Klein, 2002) and a tetrahedral-octahedral-tetrahedral (T-O-T) structure. The T-O-T structures, or layers, are electrically neutral. The clay layers are held together by van der Waals bonds (Klein, 2002).

The coordinates for the first unit-cell are given in Table 1. The coordinates are based on those given by Skipper *et al.* (1995). The starting structure used in this simulation has a unit-cell of dimensions $5.28 \times 9.14 \times 6.56$ Å. The simulation model consists of two clay layers, each containing four unit-cells in the *X*

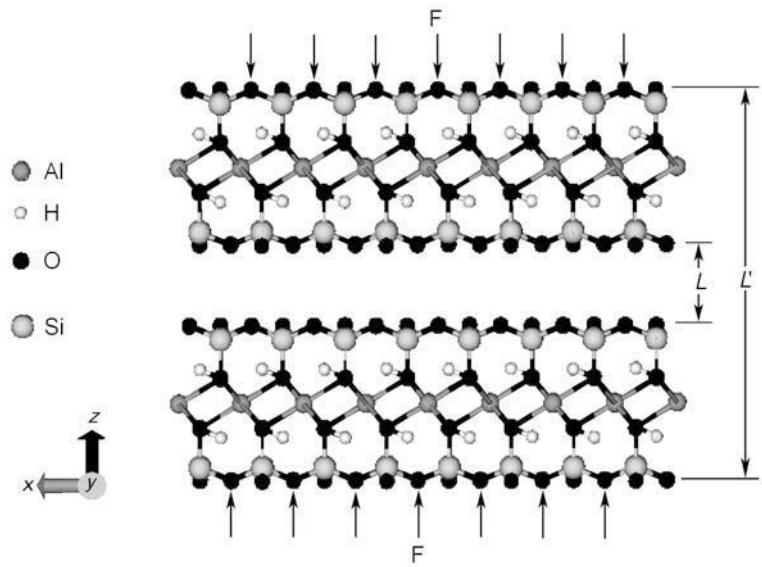

Figure 2. Forces applied normal to the simulation cell.

https://doi.org/10.1346/CCMN.2005.0530207 Published online by Cambridge University Press

direction and two unit-cells in the Y direction. The resulting overall dimensions of each clay layer are $21.12 \times 18.28 \times 6.56$ Å. The initial basal spacing and interlayer spacing of the model were 10 and 3.44 Å, respectively. The partial charges, q_i, shown in Table 1, are from Teppen *et al.* (1997). The unit-cells were patched together using PSFGEN, part of the program NAMD2.4 (Kalé *et al.*, 1999), which was developed by the Theoretical and Computational Biophysics Group in the Beckman Institute for Advanced Science and Technology at the University of Illinois at Urbana-Champaign.

SIMULATION DETAILS

For the simulations described here, the software NAMD2.4 (Kalé *et al.*, 1999) and VMD (Humphrey *et al.*, 1996), for interactive studies, were used. Simulations were run on the North Dakota State University 32 processor parallel computer system.

In the model studied, as there are two separate clay layers not connected by any real bond, a step-wise minimization procedure was followed. Each layer was minimized individually, keeping the other fixed, followed by minimization of the model as a whole. This method helps to avoid attaining a metastable state, and thus reach the lowest energy state possible with this algorithm. Individual layers were minimized for 7000 iterations, whereas for the whole model, 16,000 iterations were used. Minimization was completed several times with varying configurations. The potential energy was monitored and found to converge, so this configuration was determined to be sufficient. No constraints were used during minimization. The conjugate gradient algorithm was applied for minimization.

As it is desirable to run the simulation at atmospheric pressure and room temperature, the model was heated to 300 K followed by increasing the pressure to 1 atm. The temperature was gradually raised using the Langevin dynamics. The entire structure was heated to 350 K and cooled to 300 K twice to ensure there was no metastability. The Langevin piston method with loose coupling was used to raise the pressure to 1 atm making the model ready for performing dynamics studies.

The NAMD program uses the Verlet algorithm for the integration of MD steps. For all simulations in this work, the step size of 0.5 fs (10^{-15} s) was chosen to accommodate all possible internal interactions. All simulations were run for a total time of 200 ps (10^{-12} s) or 400,000 steps. Convergence of the total energy was reached after 200,000–250,000 steps. Periodic boundary conditions are applied with a simulation cell of dimensions $25 \times 23 \times 23$ Å. The cutoff distance used as a boundary for van der Waals interactions was 9.5 Å. Particle Mesh Ewald was used in the computation of electrostatic interaction between atom pairs. Data obtained averaging over the last 20 ps (40,000 steps) of the simulation were used to determine the positions of the atoms. Simulations took 5–6 h each using 15 processors.

FORCE-FIELD PARAMETERS

As mentioned earlier, one of the main objectives of this work was to study the force interlayer-displacement relationship. Steered MD was used, with external forces applied to each of the clay layers. For computation of the potential energy of the system, NAMD2.4 uses the CHARMm and AMBER force fields only. A search of the literature revealed that for pyrophyllite and mont-

Table 1. Coordinates for one unit-cell of pyrophyllite (based on Skipper *et al.*, 1995) and charges (Teppen *et al.*, 1997).

No.	Atom	x (Å)	y (Å)	z (Å)	q_i	No.	Atom	x (Å)	y (Å)	z (Å)	q_i
1	AL1	−0.593	−2.708	0	1.68	21	O13	3.807	−1.178	−1.06	−0.91
2	H1	3.809	0.342	1.434	0.4	22	O14	1.167	−2.708	−1.06	−0.91
3	O1	2.927	0.342	1.06	−0.96	23	O15	−0.153	−1.938	−3.28	−0.7
4	H2	0.285	0.342	−1.434	0.4	24	SI6	1.167	−2.708	−2.73	1.4
5	O2	1.167	0.342	−1.06	−0.96	25	O16	2.487	−1.938	−3.28	−0..7
6	SI1	0.287	1.862	2.73	1.4	26	SI7	3.807	1.862	−2.73	1.4
7	O3	0.287	1.862	1.06	−0.91	27	O17	3.807	1.807	−1.06	−0.91
8	SI2	0.287	−1.178	2.73	1.4	28	O18	3.807	0.342	−3.28	−0.7
9	O4	0.287	−1.178	1.06	−0.91	29	SI8	1.167	3.392	−2.73	1.4
10	SI3	2.927	−2.708	2.73	1.4	30	O19	1.167	3.392	−1.06	−0.91
11	O5	2.927	−4.228	3.28	−0.7	31	O20	−0.153	2.632	−3.28	−0.7
12	O6	2.927	−2.708	1.06	−0.91	32	O21	1.167	4.912	−3.28	−0.7
13	O7	1.607	−1.948	3.28	−0.7	33	O22	2.487	2.632	−3.28	−0.7
14	O8	4.247	−1.948	3.28	−0.7	34	AL2	2.047	−1.178	0	1.68
15	O9	0.287	0.342	3.28	−0.7	35	AL3	2.047	1.862	0	1.68
16	SI4	2.927	3.392	2.73	1.4	36	H3	2.926	4.912	−1.434	0.4
17	O10	2.927	3.392	1.06	−0.91	37	O23	3.807	4.912	−1.06	−0.96
18	O11	1.607	2.622	3.28	−0.7	38	AL4	4.687	3.392	0	1.68
19	O12	4.247	2.622	3.28	−1.7	39	H4	1.169	−4.223	1.434	0.4
20	SI5	3.807	−1.178	−2.73	1.4	40	O24	0.287	−4.228	1.06	−0.96

https://doi.org/10.1346/CCMN.2005.0530207 Published online by Cambridge University Press

Table 2. Conversion of Teppen *et al.* (1997) bonded parameters to CHARMm functionality.

Bond stretching			Teppen *et al.* (1997)			CHARMm	
i	*j*	r_0	k_2^B (kcal/mol Å^2)	k_3^B (kcal/mol Å^3)	k_4^B (kcal/mol Å^4)	k^B (kcal/mol Å^2)	R^2
ao	ocl	1.955	328.700	341.000	2189.000	382.617	0.975
ocl	hcl	0.988	656.800	−1627.500	3684.200	827.209	0.876
sz	oss	1.626	459.100	−672.400	443.400	492.387	0.935
sz	ocl	1.62	494.100	−36.700	2150.700	558.593	0.995

Angle bending				Teppen *et al.* (1997)			CHARMm	
i	*j*	*k*	θ_0	k_2^A (kcal/mol rad^2)	k_3^A (kcal/mol rad^3)	k_4^A (kcal/mol rad^4)	k^A (kcal/mol rad^2)	R^2
ao	ocl	hcl	118	44.000	−53.400	103.400	34.933	0.968
sz	ocl	ao	124.5	195.300	48.900	185.300	155.754	0.988
oss	sz	ocl	110.6	88.100	−57.000	92.500	97.493	0.900
ao	ocl	ao	109.5	195.300	48.900	185.300	198.270	0.998
ocl	ao	ocl	90/180	−40.000	0.000	32.400	80.000	0.957

Torsion					Teppen *et al.* (1997)			CHARMm	
i	*j*	*k*	*l*	φ_{0n}	V_1^D (kcal/mol)	V_2^D (kcal/mol)	V_3^D (kcal/mol)	V^D (kcal/mol)	R^2
oss	sz	ocl	ao	0	0.160	1.790	0.200	0.722	0.589

Atom type descriptions
ao Al in octahedral sheet
ocl O in octahedral sheet (in coordination with Al)
hcl H in the octahedral sheet (OH group)
sz Si in the tetrahedral sheet
oss surface O

morillonite, parameters are not available for these two particular force fields. Parameters have been developed by Teppen *et al.* (1997) for the consistent force field, CFF (Maple *et al.*, 1994). One part of this study is to calculate CHARMm parameters to extend use of steered MD for clays. With these parameters available, the steered MD becomes a potential tool for studying the mechanical response of smectite clays, clay surfaces and interlayers. In this work, force-field parameters were transcribed from CFF functionality to CHARMm functionality using the parameters developed by Teppen *et al.* (1997). The average correlation coefficient obtained between the CFF and CHARMm force fields for bond, angle, dihedral and non-bonded parameters are shown in Tables 2 and 3. Bond energy is the energy due to stretching of the bond between two atoms. Angle energy is the energy from bending the angle formed by three atoms. Dihedral energy is the energy taken to bend the dihedral angle (or torsion angle) formed by four bonded atoms.

The potential energy expression for CFF (Teppen *et al.*, 1997) is given in equation 1,

$$E_{\text{potential}} = \sum_{\text{bond}} \left[k_2^B(r-r_0)^2 + k_3^B(r-r_0)^3 + k_4^B(r-r_0)^4\right] + \sum_{\text{angle}} \left[k_2^A(\theta-\theta_0)^2 + k_3^A(\theta-\theta_0)^3 + k_4^A(\theta-\theta_0)^4\right] + \sum_{\text{dihedral}} \sum_{n=1}^{3} V_n^D[1+\cos(n\varphi-\varphi_{0n})] + \sum_{\text{vanderWaals}} \sum_{i\neq j} \left[\frac{A_i A j}{r_{ij}^9} - \frac{B_i B_j}{r_{ij}^6}\right] + \sum_{\text{electrostatic}} \sum_{i\neq j} \frac{q_i q_j}{r_{ij}} \quad (1)$$

where k_i^B, r_0, k_i^A, θ_0, V_n^D, φ_{0n}, A_i, A_j, B_i, B_j and q_i are the force field parameters obtained from experimental results, *ab initio* calculations, *etc.* r, θ, φ and r_{ij} are the bond length, bond angle, dihedral angle, and distance between two non-bonded atoms, respectively, for each

Table 3. Conversion of Teppen *et al.* (1997) non-bonded parameters to CHARMm functionality.

i	A_i ((kcal/mol) Å $^9)^{1/2}$	B_i ((kcal/mol) Å $^6)^{1/2}$	σ (kcal/mol)	ε (Å)
sz	775.000	0.010	0.001	7.400
ocl	790.000	190.000	6.000	2.800
ao	2800.000	0.010	0.150	6.300
oss	635.000	140.000	1.000	3.000
hcl	2.000	0.400	0.0001	2.400

https://doi.org/10.1346/CCMN.2005.0530207 Published online by Cambridge University Press

time step, q_i is the partial charge of each atom. Energy due to bond stretching is summed over every pair of bonded atoms and likewise for each term in the equation.

The energy in CHARMm (Brooks *et al.*, 1983) force field is shown in equation 2,

$$E_{\text{potential}} = \sum_{\text{bond}} k^B(r - r_0)^2 + \sum_{\text{angle}} k^A(\theta - \theta_0)^2 + \sum_{\text{dihedral}} V^D[1 + \cos(n\varphi - \delta)] + \sum_{\text{vanderWaals}} \sum_{i \neq j} 4\varepsilon_{ij}\left[\left(\frac{\sigma_{ij}}{r_{ij}}\right)^{12} - \left(\frac{\sigma_{ij}}{r_{ij}}\right)^{6}\right] + \sum_{\text{electrostatic}} \sum_{i \neq j} \frac{q_i q_j}{r_{ij}} \quad (2)$$

where k^B, r_0, k^A, θ_0, V^D and q_i are as explained in the previous equation. δ is the phase angle. σ_{ij} and ε_{ij} are the standard Lennard-Jones potential parameters.

From the available parameters of Teppen *et al.* (1997), energy for each bond, angle, dihedral and van der Waals pair has been calculated within a certain range (8–10%) of reference value. Regression analysis has been performed on values from the CFF energy equation for bond, angle, dihedral, and van der Waals interactions using the CHARMm equation to evaluate parameters for NAMD. The results obtained from this analysis for the bonded and non-bonded parameters are given in Tables 2 and 3, respectively. The average correlation coefficient obtained for the non-bonded parameters is 0.95.

At the middle of the clay layer, Al is octahedrally coordinated by O. In this sheet, the angle formed by O–Al–O can be either 90º or 180º. As shown in Figure 3, the higher-order terms in CFF and the parameters developed by Teppen *et al.* (1997) allow for the angle ocl–ao–ocl to have two minima, one at 90º and another at 180º. This CFF feature cannot be directly incorporated in CHARMm. Therefore it was necessary to introduce three atom types for octahedral O in place of ocl. The new atom types are oa, ob and oc. When like atoms exist on opposite sides of Al, the reference angle of 180º is used. For unlike atoms, the reference angle is 90º. Thus, two separate correlations were made between CFF and CHARMm about these minima with a reasonable deviation in each case. Since the parameters developed by Teppen *et al.* (1997) are symmetrical, the correlation about 90º and 180º is the same. The resulting k for both angles is 80.000 as shown in Table 2.

The correlation between CHARMm and the Teppen *et al.* (1997) parameter for ocl–hcl bond stretching is lower than that of most other parameters examined. The higher-order terms in the CFF bond-stretching function help achieve a better fit to experiment than can be achieved by CHARMm. However, within the region closest to the reference value, the two functions match very well as seen in Figure 4. It is also important to realize that the current study is a correlation between CHARMm and the parameters developed by Teppen *et al.* (1997), not experiment.

In Teppen *et al.* (1997), the dihedral energy corresponding to oss–sz–ocl–ao is the only dihedral energy to have non-zero force constants. The force constants for all other dihedral energies are therefore not shown in the table. The correlation obtained between the CHARMm and CFF energy functions for this dihedral energy (0.589) is not as high as that computed for other energies. However, as the force constants for this term are low, the contribution to the total energy is small, and there is little effect on the overall results. As will be seen in the next section, the results of this study are unaffected by this parameter.

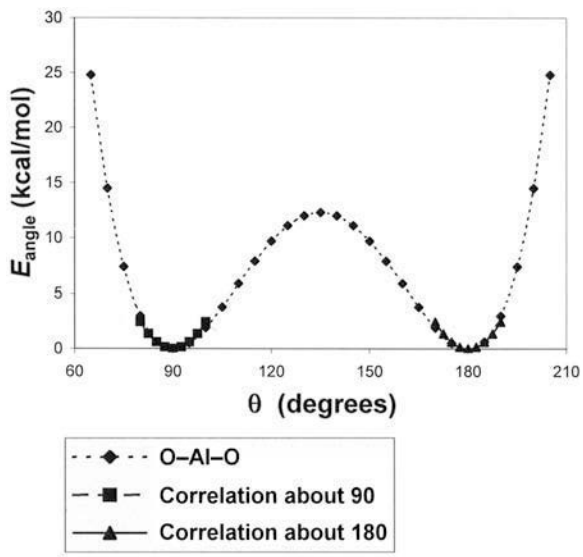

Figure 3. Correlations for O–Al–O angle bending (ocl–ao–ocl) about minima at 90º and 180º.

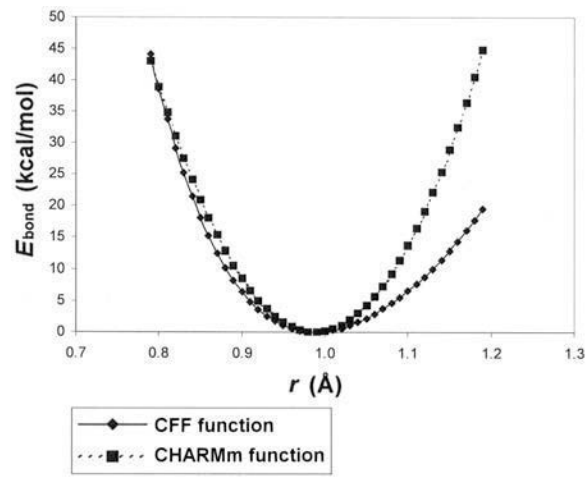

Figure 4. Bond-stretching energy *vs.* O–H bond length (ocl–hcl).

https://doi.org/10.1346/CCMN.2005.0530207 Published online by Cambridge University Press

Table 4. Comparison of unit-cell dimensions and O–H bond length.

	Present work	Wardle and Brindley (1972)	Lee and Guggenheim (1981)	Refson *et al.* (2003)	Stackhouse *et al.* (2001)	Sainz-Diaz *et al.* (2001)
a (Å)	5.60	5.161	5.160	5.218	5.15	5.14
b (Å)	9.78	8.957	8.966	9.079	8.93	9.06
c (Å)	10.48	9.351	9.347	10.001	13.17	8.14
α (°)	87.96	91.03	91.18	90.491	90.5	91.6
β (°)	99.19	100.37	100.46	101.727	99.2	101.8
γ (°)	89.68	89.75	89.64	89.687	89.7	89.7
O–H (Å)	0.98				0.9695	

RESULTS AND DISCUSSION

Forces were applied to the surface O atoms ranging from 0 pN to 160 pN, as illustrated in Figure 2. Given the surface area of the clay layers and the number of O atoms to which force has been applied, the equivalent stress can be found. The stress on the surface of each clay layer ranged from 0 to 1.65 GPa. The basal spacing, interlayer spacing, layer thickness, bond lengths and angles were monitored. Initially simulations were repeated three times to establish the expected variability in MD. Interlayer spacing varied by as much as 0.06 Å, or 1.5%.

The unit-cell parameters found for the model after running with no applied force for 200,000 ps are given in Table 4. Results from X-ray diffraction (Wardle and Brindley, 1972; Lee and Guggenheim, 1981), *ab initio* (Refson *et al.*, 2003; Stackhouse *et al.*, 2001), and empirical potentials (Sainz-Diaz *et al.*, 2001) are also shown in Table 4. The unit-cell parameters obtained from this study are dependent on three factors, the starting coordinates (Skipper *et al.*, 1995), the reference values and CFF parameters (Teppen *et al.*, 1997), and the quality of the correlations to those parameters found here. Considering these factors, the results seem to be within a reasonable range of the results given by others.

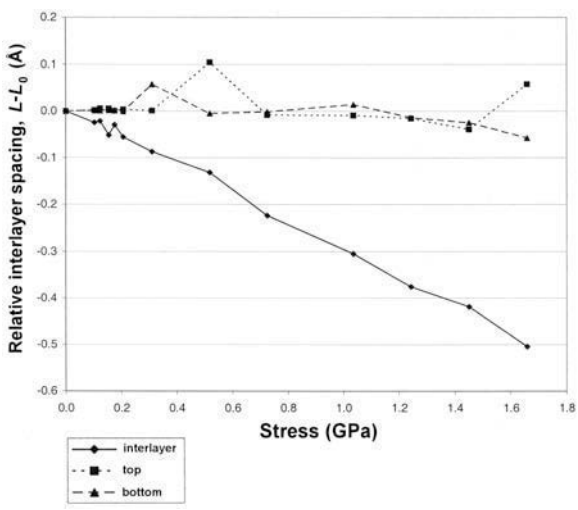

Figure 5. Applied stress *vs*. relative interlayer spacing, $L-L_0$, and relative layer thickness.

As stated previously, the R^2 value for the ocl–hcl bond was not as high as that of most other parameters. Using the parameters developed here for CHARMm, the average O–H bond length (Table 4) measures 0.98 Å, with only a 0.01 Å difference between it and the results obtained by Stackhouse *et al*. (2001).

Figure 5 shows the relationship between stress and interlayer spacing. As the stress applied to the surface of each clay layer is increased, the interlayer distance decreases almost linearly.

Also shown in Figure 5 is the thickness of the top and bottom clay layers with increasing compressive stress. As increasing stress is applied, the layer thickness is relatively unchanged. The maximum variation of layer thickness over the range of 0–1.65 GPa applied is ~1.6%. This is fairly small compared to a change of 12.9% in the interlayer spacing over the same range of stresses. Likewise, the bond lengths and angles only varied by a maximum of 4.3% from the equilibrium values. As stated above, the model was subjected to a stress range of 0 to 1.65 GPa, a large range, thus ensuring applicability of results to most practical problems.

A plot of stress *vs*. 'interlayer strain' ($\Delta L/L$) is shown in Figure 6. The 'interlayer strain' is the relative change in interlayer spacing. This is analogous to strain in a solid, but was calculated for the void space between clay layers. The stress-strain relationship as seen here is nearly linear. The relationship can be represented by the linear equation 3:

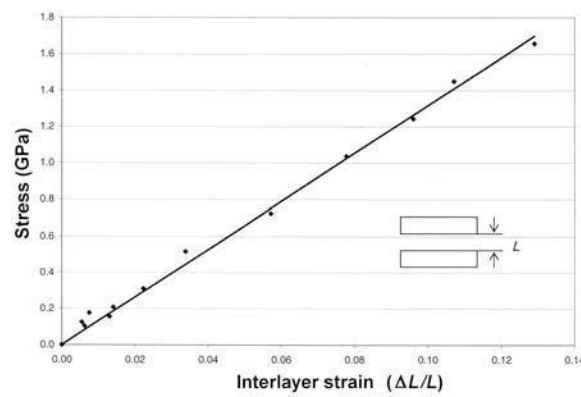

Figure 6. Stress *vs*. 'interlayer strain' ($\Delta L/L$).

https://doi.org/10.1346/CCMN.2005.0530207 Published online by Cambridge University Press

$$\sigma_v = c_v^i \varepsilon_v^i \quad (3)$$

where σ_v, c_v^i and ε_v^i are the applied stress, interlayer modulus and interlayer strain. In the case of the interlayer c_v^i = 13.18 GPa. For an applied force of 0.001 pN to ~0.1 pN magnitude, which is a fairly small force for steered MD, both positive and negative displacements were observed. For these simulations with the same low force, the average strains were found to be negative. This is believed to be a computational artifact rather than the actual material response. As indicated before, the model was fully minimized as verified by monitoring the potential energy. At larger forces, >0.1 pN, the model response is compressive, as expected. Multiple simulations at higher loads show very little variation in strain.

In Figure 7 the stress-strain curve for the entire model is shown. Although the change in layer thickness is observed to be small compared to the change in interlayer spacing, the deformation of the clay layers is measurable.

The modulus for the two-clay-layer unit, c_v^c, as illustrated in Figure 7 is 54.56 GPa. As stated earlier, the coordinates of O atoms on the surfaces of the clay layers were used to determine the thickness of the clay layers and the interlayer. The clay layers are very stiff and the interlayer undergoes most of the compression. In nature, stacks of multiple clay layers form. Understanding the behavior of the clay layers and interlayer, the modulus of these stacks of clay layers can be calculated. Averaging the thickness of the top and bottom clay layers gives a reasonable estimate of the thickness of the third layer. The thickness of the second interlayer is assumed to behave similarly to the first. The modulus for a three-clay-layer unit is calculated to be 45.26 GPa. This is the composite of the modulus of the stiff clay layers and the compressible interlayer. When larger models are considered, the modulus can be expected to decrease, as the ratio of clay layers to interlayers approaches 1:1.

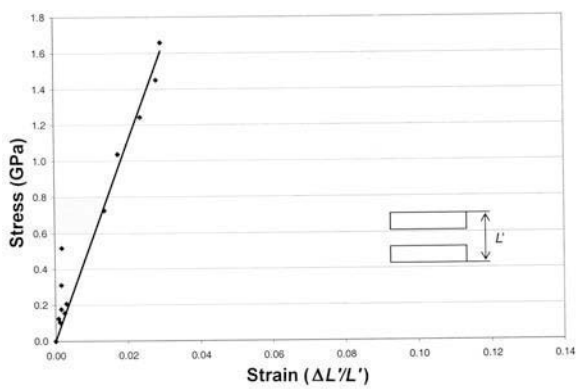

Figure 7. Stress *vs*. strain for the entire model, ($\Delta L'/L'$).

CONCLUSIONS

An atomic model for the interlayer of pyrophyllite clay has been constructed. CHARMm force-field parameters for pyrophyllite have been developed and used in conjunction with the molecular dynamics software NAMD. Steered molecular dynamics simulations on dry pyrophyllite interlayer were conducted to evaluate quantitatively the stress deformation response of the interlayer. Our results indicate that under applied compressive stress of 0 to 1.65 GPa, the stress deformation response of the interlayer is almost linear. The predominant deformation of the clay model results from deformation of interlayer spacing. Deformation of the clay layers observed in this stress range is only ~1.6% compared to ~12.9% for the interlayer. The compressive response of individual components, the clay layers and interlayer were found. The modulus of the interlayer and the two-clay-layer unit were found to be 13.18 GPa and 54.56 GPa, respectively. In this work, the steered MD is shown to be a powerful tool in evaluating the quantitative mechanical response of clay interlayers.

ACKNOWLEDGMENTS

This research was partially funded by NSF CMS grant #0114622. The cognizant program manager is Dr Richard Fragaszy. The hardware and software support for NAMD at NDSU provided by Dr Gregory Wettstein is acknowledged.

REFERENCES

Anderson, M. and Lu, N. (2001) Role of microscopic physicochemical forces in large volumetric strains for clay sediments. *Journal of Engineering Mechanics, ASCE*, **127**, 710–719.

Brooks, B.R., Bruccoleri, R.E., Olafson, B.D., States, D.J., Swaminathan, S. and Karplus, M.J. (1983) CHARMM: A program for macromolecular energy, minimization, and dynamics calculations. *Journal of Computational Chemistry*, **4**, 187–217.

Capkova, P., Driessen, R.A.J., Numan, M., Schenk, H., Weiss, Z. and Klika, Z. (1998) Molecular simulations of montmorillonite intercalated with aluminum complex cations. Part II: Intercalation with $Al(OH)_3$-fragment polymers. *Clays and Clay Minerals*, **46**, 240–244.

Chang, F.-R., Skipper, N.T. and Sposito, G. (1995) Computer simulation of interlayer molecular structure in sodium montmorillonite hydrates. *Langmuir*, **11**, 2734–2741.

Chang, F.-R., Skipper, N.T. and Sposito, G. (1998) Monte Carlo and molecular dynamics simulations of electrical double-layer structure in potassium-montmorillonite hydrates. *Langmuir*, **14**, 1202–1207.

Chen, J., Anandarajah, A. and Inyang, H. (2000) Pore fluid properties and compressibility of kaolinite. *Journal of Geotechnical and Geoenvironmental Engineering, ASCE*, **126**, 798–807.

Greathouse, J.A., Refson, K. and Sposito, G. (2000) Molecular dynamics simulation of water mobility in magnesium-smectite hydrates. *Journal of the American Chemical Society*, **122**, 11459–11464.

Humphrey, W., Dalke, A. and Schulten, K. (1996) VMD – Visual Molecular Dynamics. *Journal of Molecular*

https://doi.org/10.1346/CCMN.2005.0530207 Published online by Cambridge University Press

Graphics, **14**, 33–38. http://www.ks.uiuc.edu/Research/vmd/

Hwang, S., Blanco, M., Demiralp., E., Cagin, T. and Goddard, W.A. (2001) MS-Q force field for clay minerals: application to oil production. *Journal of Physical Chemistry B*, **105**, 4122–4127.

Jo, H.Y., Katsumi, T., Benson, C. and Edil, T.B. (2001) Hydraulic conductivity and swelling of nonprehydrated GCLs permeated with single species salt solutions. *Journal of Geotechnial and Geoenvironmental Engineering, ASCE*, **127**, 557–560.

Kalé, L., Skeel, R., Bhandarkar, M., Brunner, R., Gursoy, A., Krawetz, N., Phillips, J., Shinozaki, A., Varadarajan, K. and Schulten, K. (1999) NAMD2: Greater scalability for parallel molecular dynamics. *Journal of Computational Physics*, **151**, 283–312. http://www.ks.uiuc.edu/Research/namd/

Katti, D. and Shanmugasundaram, V. (2001) Influence of swelling on the microstructure of expansive clays. *Canadian Geotechnical Journal*, **38**, 175–182.

Karaborni, S., Smit, B., Heidug, W., Urai, J. and van Oort, E. (1996) The swelling of clay: molecular simulations of hydration of montmorillonite. *Science*, **271**, 1102–1104.

Klein, C. (2002) *Mineral Science.* John Wiley & Sons, New York.

Lee, J.H. and Guggenheim, S. (1981) Single crystal X-ray refinement of pyrophyllite-1*Tc*. *American Mineralogist*, **66**, 350–357.

Maple, J.R., Hwang, M.-J., Stockfish, T.P., Dinur, U., Waldman, M., Ewig, C.S. and Hagler, A.T. (1994) Derivation of class-II force-fields. 1. Methodology and quantum force-field for the alkyl functional-group and alkane molecules. *Journal of Computational Chemistry*, **15**, 162–182.

McBride, M.B. (1994) *Environmental Chemistry of Soils.* Oxford University Press, New York.

Newman, S.P., Christina, T.D., Coveney, P.V. and Jones, W. (2002) Molecular dynamics simulation of cationic and anionic clays containing amino acids. *Langmuir*, **18**, 2933–2939.

Refson, K., Park, S.-H. and Sposito, G. (2003) *Ab initio* computational crystallography of 2:1 clay minerals: 1. Pyrophyllite-1*Tc*. *Journal of Physical Chemistry B*, **107**, 13376–13383.

Sainz-Diaz, C.I., Hernández-Laguna, A. and Dove, M.T. (2001) Modeling of dioctahedral 2:1 phyllosilicates by means of transferable empirical potentials. *Physics and Chemistry of Minerals*, **28**, 130–141.

Shroll, R.M. and Smith, D.E. (1999) Molecular dynamics simulations in the grand canonical ensemble: Application to clay mineral swelling. *Journal of Chemical Physics*, **111**, 9025–9033.

Skipper, N.T., Sposito G. and Chang, F.-R. (1995) Monte Carlo simulations of interlayer molecular structure in swelling clay minerals. 1. Methodology. *Clays and Clay Minerals*, **43**, 285–293.

Smith, D.E. (1998) Molecular computer simulations of the swelling properties and interlayer structure of cesium montmorillonite. *Langmuir*, **14**, 5959–5967.

Stackhouse, S., Coveney, P.V. and Sandré, E. (2001) Plane-wave density functional theoretic study of formation of clay-polymer nanocomposite materials by self-catalyzed in situ intercalative polymerization. *Journal of the American Chemical Society,* **123**, 11764–11774.

Teppen, B.J., Rasmussen, K., Bertsch, P.M., Miller, D.M. and Schafer, L. (1997) Molecular dynamics modeling of clay minerals. 1. Gibbsite, kaolinite, pyrophyllite, and beidellite. *Journal of Physical Chemistry B*, **101**, 1579–1587.

Wardle, R. and Brindley, G.W. (1972) The crystal structure of pyrophyllite, 1Tc, and of its dehydroxylate. *American Mineralogist*, **57**, 732–750.

Warne, M.R., Allan, N.L. and Cosgrove, T. (2000) Computer simulation of water molecules at kaolinite and silica surfaces. *Physical Chemistry Chemical Physics*, **2**, 3663–3668.

(*Received 24 April 2004; revised 24 September 2004; Ms. 907; A.E. Randall T. Cygan*)